Eur. Phys. J. D **45**, 439–446 (2007)
DOI: 10.1140/epjd/e2007-00170-1

THE EUROPEAN PHYSICAL JOURNAL D

Self-assembly of Mo_6S_8 clusters on the Au(111) surface

I. Popov[1,a], T. Kunze[1,2], S. Gemming[1,3,b], and G. Seifert[1,c]

[1] Physikalische Chemie, TU Dresden, 01062 Dresden, Germany
[2] Institute of Physics, TU Chemnitz, 09107 Chemnitz, Germany
[3] Institute of Ion Beam Physics and Materials Research, FZ Dresden-Rossendorf, P.O. Box 510119, 01314 Dresden, Germany

Received 30 January 2007
Published online 23 May 2007 –

Abstract. The preferred adsorption sites and the propensity for a self-organised growth of the molybdenum sulfide cluster Mo_6S_8 on the Au(111) surface are investigated by density-functional band-structure calculations with pseudopotentials and a plane wave basis set. The quasi-cubic cluster preferentially adsorbs via a face and remains structurally intact. It experiences a strong, mostly non-ionic attraction to the surface at several quasi-isoenergetic adsorption positions. A scan of the potential energy surface exhibits only small barriers between adjacent strong adsorption sites. Hence, the cluster may move in a potential well with degenerate local energy minima at room temperature. The analysis of the electronic structure reveals a negligible electron transfer and S-Au hybridised states, which indicate that the cluster-surface interaction is dominated by S-Au bonds, with minor contributions from the Mo atom in the surface vicinity. All results indicate that Mo_6S_8 clusters on the Au(111) surface can undergo a template-mediated self-assembly to an ordered inorganic monolayer, which is still redox active and may be employed as surface-active agent in the integration of noble metal and ionic or biological components within nano-devices. Therefore, a classical potential model was developed on the basis of the DFT data, which allows to study larger cluster assemblies on the Au(111).

PACS. 61.46.-w Nanoscale materials – 73.22.-f Electronic structure of nanoscale materials: clusters, nanoparticles, nanotubes, and nanocrystals – 72.20.-i Conductivity phenomena in semiconductors and insulators

1 Introduction

Depending on their size and composition molybdenum sulfide particles serve various key applications as solid lubricant [1], electrode contact material [2], or dehydrosulphurisation catalyst [3]. Bulk MoS_2 is a semi-conducting lubricant of fairly low catalytic activity, which consists of weakly bonded units of sulphur-molybdenum-sulphur trilayers that can easily glide on each other [4]. However, the smallest units of MoS_2 that remain stable when they are absorbed onto gold are actually sulphur-deficient clusters with up to six Mo atoms, each containing a sulphur-decorated metalloid core [5,6]. Such clusters are produced in a pulsed arc cluster ion source and exhibit pronounced peaks in the mass spectrum which stem from Mo_4S_6, Mo_6S_8, Mo_9S_{11}, etc. clusters. The stability and structural properties of these clusters have been investigated [7–12]. For free clusters with more than three molybdenum atoms a cluster-platelet transition was found at a stoichiometry of Mo:S = 1:3, i.e. in the limit, when all molybdenum electrons are formally transferred to the sulphur sites, and no d electrons remain to make metallic Mo-Mo bonds. The Mo_6S_8 cluster investigated here is below this threshold and contains an octahedral metalloid Mo_6 cluster core decorated by sulphur atoms. The most stable small cluster is Mo_4S_6 with a large energy gap of 3 eV between the highest occupied (HOMO) and lowest unoccupied (LUMO) molecular orbital. Although experimentally abundant, the next larger stable Mo_6S_8 exhibits only a calculated HOMO-LUMO energy gap of 0.8 eV [7,13], which suggests a weaker stability, but higher reactivity than Mo_4S_6. Comparable energy gaps of up to 0.6 eV have also been obtained from DFT calculations for small, pure, Jahn-Teller distorted molybdenum clusters [14–16] and indicate a stability comparable to the one of Mo_6S_8. A major application of Mo_6S_8-containing compounds is the use as contact material in solid fuel cells, because the Mo_6S_8-based Chevrel phases may readily store or release lithium or magnesium ions [2]. Furthermore, the existence of network structures made of $[Mo_{3n}S_{3n+1}]^{d-}$ cluster anions with K, Cs, and In counter ions [17,18] indicates that the Mo_6S_8 cluster may readily assume a negatively charged state. With increasing sulphur content small clusters undergo a cluster-platelet transition to flat triangular nanoplatelets [10]. When supported on gold such platelets

[a] e-mail: igor.popov@chemie.tu-dresden.de
[b] e-mail: s.gemming@fzd.de
[c] e-mail: Gotthard.Seifert@chemie.tu-dresden.de

are excellent catalysts for the dehydrosulphurisation of fuels [19–21]; the atomistic and electronic factors of the reactivity have recently been revealed experimentally [3,22]. Theoretical and experimental investigations suggest that the flat platelets are stable under sulphur-rich preparation conditions for particle sizes of up 400–500 atoms. Larger particles exhibit three-dimensional structures; up to 25 000 atoms, those clusters assume a regular shape composed of nested octahedra, and still larger structures grow into rounded inorganic fullerenes [23,24] or even nanotubes [25,26] or nanowires [27].

Scanning tunneling microscopy images suggest an ordered growth of the sulphur rich nanoplatelets on the Au(111) surface [3], which indicates a non-negligible cluster-support interaction. Likewise, calculations showed that the magic Mo_4S_6 cluster is strongly bound on Au(111), and only internal structural relaxations are induced [6]. Recent experiments have demonstrated [28] that self-assembly may be achieved with the small molybdenum sulfide cluster $Mo_3S_4^{4+}$. In this way, redox-active, purely inorganic monolayers on the noble metal can be formed. Other recent experiments have revealed that even larger, structurally intact Mo_4S_6, Mo_6S_8, and Mo_7S_{10} clusters may be deposited on the Au(111) surface [29]. This is not the case for small pure Mo_n clusters, which undergo significant atom rearrangements and have been observed to form thiol-selective, less reactive gold-covered core-shell particles by surface alloying [30,31]. Besides the above-mentioned ion storage capacity, the high reactivity of sulphur with noble metals makes an Mo_6S_8 electrode a good contact to the external metallic wiring, such that the molybdenum sulfide layer acts as an interface-active species, which enhances the wettability and the contact quality of the fuel cell interior by the wiring. Future applications may utilise this effect for generating a structurally well-defined nano-contact. As nowadays contact geometries are still macroscopic, however, it is desirable that the clusters can self-assemble on a Au(111) template to a uniform inorganic monolayer. As the smaller cluster cation $Mo_3S_4^{4+}$ indeed forms such redox-active inorganic monolayers on length scales of up to a micron [28], the propensity of Mo_6S_8 towards template-mediated self-assembly is investigated here.

After a summary of the computational details in Section 2 the investigated model structures and the optimised geometries are given in Section 3; Section 4 describes the adsorption energetics at the optimum adhesion positions and the full potential energy surface for cluster adsorption. In Section 5 a classical potential model is derived, which allows the description of larger system sizes, such as cluster assemblies. We conclude with a short summary in Section 6.

2 Computational details

All structural, energetic, and electronic properties were obtained by density-functional band-structure calculations with the ABINIT code [32], which uses a plain-wave basis to represent the valence states and norm-conserving pseudo potentials to describe the core-valence interaction [33,34]. In detail, Troullier-Martins-type pseudopotentials for the configurations $[Kr]5s^25p^{0.5}4d^{3.5}$ of Mo $[Ne]3s^23p^{3.5}3d^{0.5}$ of S, and $[Xe]6s^{1.75}5d^{9.75}6p^{0.5}$ of Au were employed. The convergence of the k-point grid and the cutoff energy for the plane wave basis were tested for the surface energy of the substrate, the pure Au (111) surface with $4 \times 4 \times 3$ gold atoms in the supercell. The value is converged for a $(2, 2, 1)$ Monkhorst-Pack type k-point mesh and an energy cutoff of 550 eV. Thus, the Γ-point approximation has been employed during the preoptimisation of the model structures and for scanning the energy surface for the cluster-substrate interaction. The structures were optimised in a two-step procedure, employing the local density approximation [35], and a refinement was carried out at the generalised gradient approximation (Becke-Perdew) [36] level. Upon cluster adsorption, the relaxation of the Au (111) surface was restricted to the first layer, in order to simulate a semi-infinite surface. The maximum force per atom in optimised structures is 5.0×10^{-4} Ha/Bohr atom. Atomic charges were calculated by the Bader technique [37].

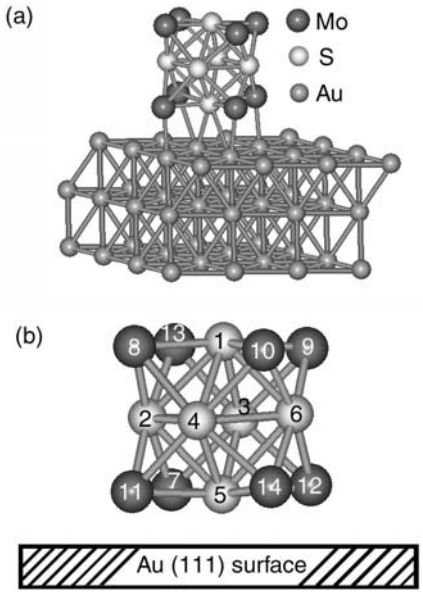

Fig. 1. (a) Adsorption of Mo_6S_8 via a face at the `square bridge` position. The Mo atom bridges two adjacent Au atoms, two S atoms adsorb on-top of Au atoms, and the two other two S atoms occupy three-fold hollow sites. (b) Schematic view with numbering of the atoms in the cluster.

3 Adsorption geometries

3.1 Model structures

As the band-structure approach employs three-dimensionally periodic boundary conditions, a repeated-slab supercell was employed, as depicted in Figure 1. The structure is composed of 48 gold atoms, 16 per layer, and the Mo_6S_8 cluster on top of the surface. The lengths of the

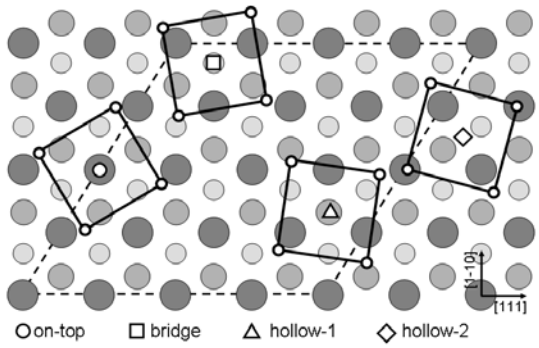

Fig. 2. Investigated adsorption positions and relative orientations of the cluster with respect to the top layer of the surface. For the `square` orientation the position of the sulphur atoms is schematically indicated by a square and the symbol in the centre denotes the molybdenum position; `tip` orientation, the sulphur atom closest to the surface is located at the position of the symbol. The supercell size is indicated by dashed lines.

hexagonal supercell lattice vectors amount to 11.538 Å in plane, and to 30.000 Åin the direction orthogonal to the gold surface. Thus, the model represents an unreconstructed Au(111) surface, which is densely covered by Mo_6S_8 clusters with inter-cluster separations of 6.17 Å to 6.60 Å and separated from the periodic replica along the surface normal by a vacuum region of more than 15 Å.

During the optimisation of the free cluster its initial O_h symmetry is lowered to near D_{2h} due to a Jahn-Teller distortion. The horizontal σ_h mirror plane of this space group is defined by the atoms 7, 10, and 13, and the vertical σ_v plane by the atoms 2, 3 and 4. The C_2 rotation axis penetrates the bond centres of the bonds between the molybdenum atoms 2 to 3 and 4 to 6. This pre-optimised cluster is placed at high-symmetry sites of the ideal gold surface with a cubic lattice constant of 4.08 Å (Fig. 2). The position of the cluster on the high-symmetry points of the surface is denoted with respect to the cluster atom, which is the closest to the surface. The following four high-symmetry positions of the Au(111) surface were studied: `On-top` of the gold atoms (circles), at the `bridge position` between two neighbouring gold atoms (squares), and at the hollow sites coordinated by three gold atoms (triangles). For the latter position a distinction is made between `hollow site 1` (black triangle), which is the hcp site with one gold atom below the adsorption site in the subsurface gold layer, and `hollow site 2` (white triangle), which is the fcc site, where the closest adsorbed cluster atom continues the ABC stacking sequence of the face-centred-cubic gold bulk.

At each position, two orientations of the cluster with respect to the surface were investigated: in the `tip` orientation, the cluster bonds via a sulphur atom at the corner of the Mo_6S_8 cluster, and the space diagonal of the cluster is orthogonal to the surface; in the `square` orientation the cluster adsorbs via a face of the Mo_6S_8 cube, such that one molybdenum atom and four sulphur atoms are situated in a plane parallel to the surface. For the `square` orientation the adsorption position is given with respect to the central molybdenum atom, whereas the surrounding four sulphur atoms must occupy different sites due to the incommensurability of the cubic cluster structure and the hexagonal atom arrangement of the Au(111) surface. Thus, the `square bridge` position of the molybdenum places two sulphur atoms on top, and the other two close to bridge sites. For the `square hollow` position, the sulphur atoms are slightly shifted away from the hollow sites. For the `square on-top` position two sulphur atoms occupy bridge sites and the other two sulphur atoms are slightly shifted from on-top sites towards the hollow sites. These site, position, and orientation definitions will be used in the following sections.

3.2 Structural properties

In order to assess the influence of the adsorption on the structural properties, a two-step optimisation protocol was carried out: first, the cluster and surface geometries were fixed at the values of the free fragments and only the cluster-surface distance was varied. Second, the geometries of the adsorbed cluster and the surface gold layer were completely optimised.

The free, unreconstructed Au(111) surface is characterised by bulk-type distances between all gold atoms. The free Mo_6S_8 cluster contains a Jahn-Teller distorted Mo_6 metal core with five short Mo-Mo bonds of about 2.60 Å and nine long bonds of about 2.70 Å. The eight faces of this core are capped by sulphur atoms at distances of 2.47 to 2.52 Å such that a distorted sulphur cube is formed with edge lengths of about 3.40 and 3.60 Å. At fixed cluster and surface geometries the optimum cluster-surface distances amount to 2.30–2.60 Å for the `square`-oriented clusters and 1.80–2.00 Å for the `tip`-oriented ones with the exception of the `tip on-top` position, whose distance amounts to 2.40 Å. After full optimisation the cluster-surface shrinks by another 0.1 Å, and both fragments undergo distortions.

First, the most stable adsorption geometries, the `square` arrangements, are discussed. At the most preferred `square bridge` adsorption position the equilibrium cluster-surface distance amounts to 2.27 Å. Thus, the two Mo-Au bonds as well as two of the four S-Au bonds assume lengths, which are very close to the respective sums of the covalent radii r_c(Mo) = 1.36 Å, r_c(S) = 1.02 Å, and r_c(Au) = 1.44 Å [38]. Structure changes occur in both fragments: the Jahn-Teller distortion of the cluster is not lifted, but all Mo-Mo distances are elongated to values between 2.70 and 2.74 Å, and also the S-S distances become more uniform with values between 3.50 to 3.60 Å. Also the gold surface atoms underneath the cluster relax by up to 0.1 Å in order to reach the most favourable bond distances. Thus, the symmetry of the adsorbed cluster is almost C_{4v} with the four-fold rotation axis parallel to the surface normal. The asymmetric relaxations indicate, that the bonding within the Mo_6S_8 cluster is slightly weakened in the contact region to the Au(111) surface, but otherwise unchanged.

For the low-symmetry `square hollow` positions the equilibrium distance between the cluster and surface amounts to 2.17 Å, which is again in good agreement with the sums of covalent radii for the Mo-Au bonds, but leads to a considerable elongation of the S-Au bonds by more than 0.1 Å even after optimisation. The geometry changes in cluster and gold surface layer are of the same character as for the `square bridge` adsorption position. At both `square hollow` positions the central molybdenum atom is located in the centre of the hollow site, and the Au-coordinated sulphur atoms exhibit shifts along the z-direction of 0.07–0.15 Å away from the surface and from the Au/coordinated molybdenum atom.

The `square on-top` position exhibits an unfavourably low Mo-Au distance of 2.624 Å, but still moderately to strongly elongated S-Au bonds. Due to the high symmetry of the adsorption position, the shifts within the Au surface are negligible. For the cluster the relaxation pattern is comparable with the one of the other `square` positions: the lower triangle of molybdenum atoms is elongated to bond lengths of 2.75 to 2.79 Å, whereas the lengths of the upper triangle all amount to 2.72 ± 0.01 Å.

For the `tip` orientation shorter cluster-surface distances were calculated, but the adsorption induced structure changes of the two fragments are lower than for the `square` orientation. The cluster assumes a symmetry very close to C_{3v}, which matches the symmetry of the surface. As for the `square` positions, the cluster atoms closer to the surface exhibit larger interatomic distances than the ones pointing away from the surface. This indicates, that also in the `tip` orientation the bonding within the cluster is slightly weakened by the interaction with the gold surface, but a Jahn-Teller distortion remains.

At the `tip on-top` position only those sulphur atoms are shifted, which are second nearest neighbors to the surface. With 2.386 Å the S-Au distance is, however, shorter than the sum of the covalent radii. In the `tip hollow` positions the gold atoms coordinated to the sulphur atom of the cluster relax away from each other and towards the cluster by 0.03–0.04 Å Due to this relaxation, the S-Au contact distances are also increased by 0.02–0.09 Å, although the cluster moves towards the surface by about 0.06 Å upon optimisation. For both adsorption positions the S-Au distances are close to the favourable range of 2.45 Å to 2.50 Å for the Au-S bond. Similar S-Au bond length values are also obtained for the `tip bridge` position, where the structural relaxation of the Au(111) surface at the bridge site is more pronounced than around the other adsorption sites.

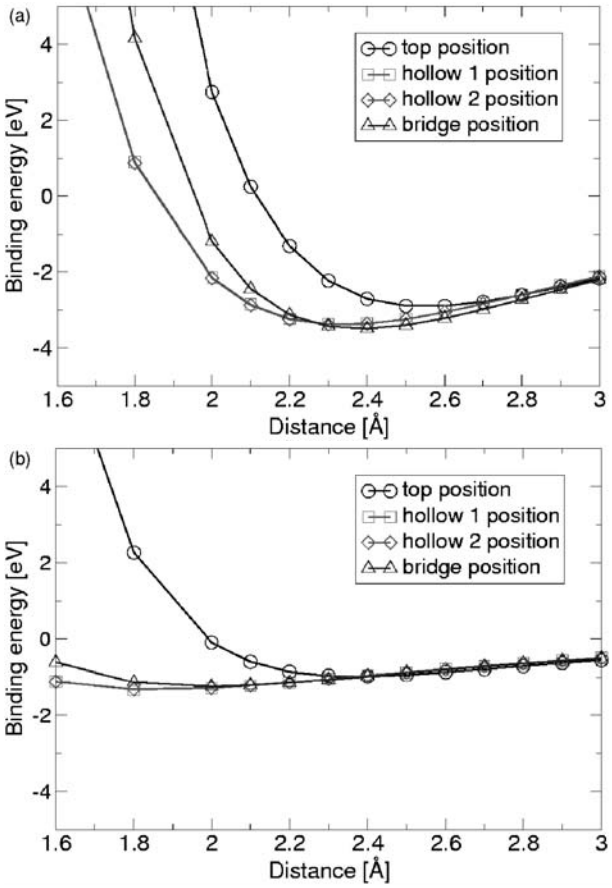

Fig. 3. Binding energies [eV] for the adsorption of the unrelaxed Mo_6S_8 cluster at the "square" (top) and "tip" (bottom) orientations as a function of the cluster-surface distance [Å] (LDA, Γ-point approximation).

4 Adsorption energetics

4.1 Binding energies at high-symmetry positions

The cluster-surface binding energy is calculated as the difference between the total energy of the whole model structure and the values of the separate Mo_6S_8 cluster and the Au(111) surface. In order to avoid numerical inaccuracies the separate fragments were calculated in the same supercell as the whole model structure. First, the dependence of the binding energy, E_{bind}, is investigated as a function of the distance between the cluster and the substrate. Figure 3 shows the binding energies for the different adsorption sites as a function of the cluster-surface distance obtained from local-density-functional calculations. Generally, the `square` orientations are by 2 eV more preferable than the `tip` ones on all positions. The difference in the binding energies between the least stable `square` and the most stable `tip` cluster orientation still amounts to 1.6 eV at the LDA level. Hence, the higher coordination number of the `square` arrangement is more favourable. The `square-bridge` position exhibits the strongest adsorption of all positions and cluster orientations. In this position, two sulphur atoms occupy on-top sites, and the other two are close to such a site. In comparison, the `square on-top` position is considerably less stable by 0.6 eV. Thus, the adsorption of the cluster on top of a gold atom via a direct molybdenum gold interaction is unfavourable for a good cluster-surface binding. This finding underlines the importance of the gold-sulphur interaction for the cluster-surface bonding. An adsorption of the cluster via the `tip`

orientations is energetically favourable at the LDA level, with binding energies of about 1.2 eV.

The structures corresponding to the minima of these curves were chosen as initial structures for a full structural optimisation. After a full optimisation of the adsorbed cluster and the first layer of the Au(111) surface the `square-bridge` position remains the most favourable one with a binding energy of $E_{bind} = 4.07$ eV. At the `square hollow 1` and `square hollow 2` positions the cluster binds with 3.94 eV, and 3.97 eV, respectively, the `on-top` position is again less favourable by about 0.6 eV. The two `hollow sites` are energetically degenerate, which suggests that the gold atoms of the subsurface layer do not participate in the binding such that the interaction mechanism is confined to the gold surface layer. The difference between the binding energies of optimised `square`- and `tip`-oriented structures is in the range 1.45–2.63 eV, hence the adsorption via a face of the cluster remains the most stable arrangement after optimisation. After refinement of these results at the GGA level the binding energies are reduced by 0.75–2.53 eV and the potential energy landscape is less strongly corrugated. As the major findings are not changed by the GGA refinement, the LDA was employed for the more detailed structure investigations described below.

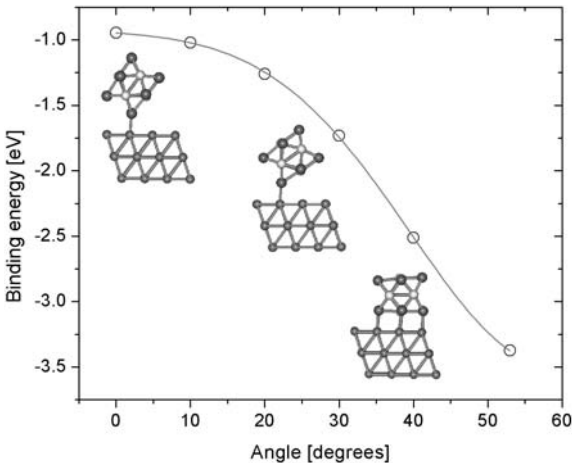

Fig. 4. Binding energy [eV] of Mo_6S_8 as a function of the rotation angle [degrees] for the transition from the `tip-top` to the `square-bridge` position as depicted by the sketches of the adsorption geometry.

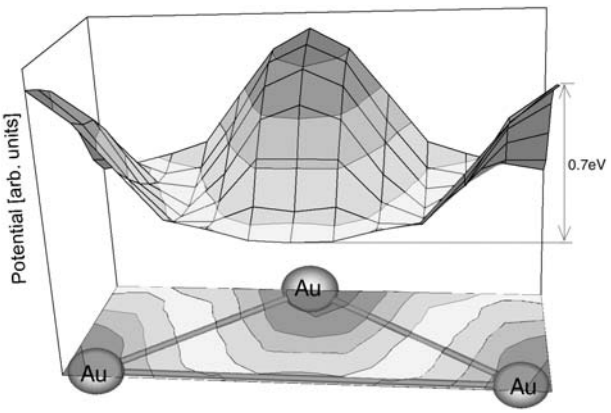

Fig. 5. Potential energy surface for the lateral motion of Mo_6S_8 on Au(111), both as three- and two-dimensional representation. The x and y coordinates specify the position of the central Mo atom with respect to the Au atoms of the surface, as drawn schematically in the lower part of the figure. At each position the rotation state with respect to the surface normal was optimised, and the cluster-surface distance was interpolated from the values at the nearest high-symmetry sites.

4.2 Potential energy surface

The propensity for the formation of self-assembled monolayers may be investigated by calculating the potential hyper-surface, which constrains the free mobility of the cluster after deposition on the surface. In the following we assume that the vibrational degrees of freedom may be neglected due to the strong cluster-surface interaction. From the remaining six rotational and translational degrees the vertical translation of the cluster along the surface normal has already been discussed above.

Two rotational degrees can transform the cluster from a `square`-oriented adsorption position to a `tip`-oriented one. As all `tip`-oriented adsorption sites are considerably less stable than the `square`-oriented ones such a geometry change is not very likely to occur, even at room temperature. Nevertheless, one such rotation from the `square` to the `tip` orientation has been examined, because there may exist additional metastable intermediates during the cluster deposition. By this transition the most unfavourable `tip on-top` position, can be transformed into the most preferred `square bridge` position by rotation of the cluster as shown in Figure 4. From the initial `tip` orientation, the cluster is first rotated around the surface normal by 30 degrees, and then rotated into the `square bridge` position around the lower sulphur atom. The obtained binding energy curve is given in Figure 4 as a function of the tilt angle. The monotonous decrease of the slope shows that no intermediate adsorption geometries occur as stable local minima, but that the system strongly prefers the `square`-oriented adsorption on the bridge site.

Thus, from the six degrees of freedom, only three are relevant for the mobility of the cluster: the lateral translations parallel to the surface and the rotation around an axis parallel to the surface normal. The vertical translation, i.e. the cluster-surface distance, is chosen as linear interpolation between the respective optimised values at the high-symmetry positions. The remaining four-dimensional potential surface was rastered in small steps by Γ-point calculations. At each lateral step the cluster was rotated around an axis parallel to the surface normal, which penetrates the centre of mass of the cluster. For a better graphical representation we restrict the dimensionality further and depict only the minimum energy for the optimum rotational angle in Figure 5 as a function of the position on the Au(111) surface, both as a contour plot and as full three-dimensional surface. The triangle at the bottom of the figure represents a part of the gold surface, with

Table 1. Fit parameters of the Gupta potential: A and B [Ha], p and q [dimensionless] as determined for the six pair potentials from fits to DFT reference structures.

	V(Mo−Mo)	V(S−S)	V(Mo−S)	V(Mo−Au)	V(S−Au)	V(Au−Au)
A	4.474	0.517	0.124	0.004	1.493	0.551
B	4.680	0.779	0.394	0.016	1.505	0.638
p	4.479	5.411	7.061	9.252	5.431	5.635
q	4.288	3.842	2.216	2.683	5.393	4.850

three gold atoms in the corners. The minima of the energy surface are located at the `bridge` positions, and maxima of 0.6 eV (LDA) or 0.2 eV (GGA) occur at the `on-top` positions. The trajectory between two neighbouring `bridge` positions crosses a relatively small (about 0.1 eV) potential barrier. Thus, at room temperature one can expect, that the clusters can move from one `bridge` position to the neighbouring one across the `hollow site` positions in-between, and that the cluster may dwell temporarily in these other local minima. Due to the larger height of the `on-top` potential barrier the diffusion on the surface has mostly translational character along the potential well, and rotational character around a surface normal which penetrates the centre of mass of the cluster. The cluster remains `square` oriented, because the rolling motion of the cluster on the surface is energetically not favourable.

5 Classical model for the self-assembly

The propensity of Mo_6S_8 clusters to form self-assembled layers must be discussed in comparison with recent experimental evidence for self-organised growth of redox-active inorganic monolayers from small sulphur-poor $Mo_3S_4^{4+}$ clusters on the Au(111) surface [28]. The local adsorption geometry via three sulphur atoms at Au-Au-bridging sites suggested for $Mo_3S_4^{4+}$ on the basis of conductivity and atomic force microscopy measurements is in very good agreement with previous results we obtained for the Mo_4S_6 cluster on Au(111). As Mo_4S_6 is structurally closely related to $Mo_3S_4^{4+}$ by the exchange of the central η^3-bound sulphur atom with an MoS_3 moiety, the experiment indicates, that also Mo_4S_6 may self-assemble to stable inorganic monolayers on the Au(111) surface. However, the large HOMO-LUMO gap (3 eV) of the Mo_4S_6 cluster, lets expect only a low redox activity, thus Mo_4S_6 may more readily be employed as an inorganic template layer for the nano-structured integration of gold and biological components. The Mo_6S_8 cluster investigated here has a smaller band gap of only 0.8 eV, hence regular Mo_6S_8 monolayers might be better candidates for redox active inorganic layers such as the nanoplatelets [39]. As the incommensurability of the cuboid Mo_6S_8 cluster and the trigonal Au(111) surface makes most of the high-symmetry adsorption sites energetically degenerate. The small barriers in-between allow the cluster to freely move in a potential well, assuming different rotation states with respect to the surface normal. In this way, the adsorbed Mo_6S_8 clusters are more free to rearrange to a structurally uniform monolayer than the trigonal Mo_4S_6 clusters.

However, less regular assemblies of molybdenum sulphide nanoparticles on the gold surface occur during the deposition and self-organisation process, which require too large supercells for a routine treatment at the full density-functional level. Furthermore, a Bader analysis of the electron redistribution upon cluster adsorption shows that no net charge transfer occurs between cluster and surface. Within the Mo_6S_8 cluster only small Bader partial charges of up 0.14 electrons are obtained and these partial charges induce even smaller, negligible image charges in the first surface layer of the Au slab. Hence the interactions within this system may be re-expressed in terms of classical two-centre and three-centre contributions.

Gold nanostructures have been successfully modelled by Gupta-type potentials with a repulsive short-range term $V_{\rm rep}$ and an attractive term $V_{\rm attr}$ at intermediate range:

$$V_{\rm c} = \sum_{i=1}^{N} \left[V_{\rm rep}\left(r_{ij}\right) - V_{\rm attr}\left(r_{ij}\right) \right], \tag{1}$$

where

$$V_{\rm rep}(r_{ij}) = \sum_{j=1;j\neq i}^{N} \left[A \exp\left(-p \left(\frac{r_{ij}}{r_0} - 1 \right) \right) \right] \tag{2}$$

and

$$V_{\rm attr}(r_{ij}) = \sqrt{\sum_{j=1;j\neq i}^{N} \left[B^2 \exp\left(-2q \left(\frac{r_{ij}}{r_0} - 1 \right) \right) \right]}. \tag{3}$$

The potential minimum $V_{\rm min}$ is numerically defined as $V_{\rm min} = |B| - |A|$ and is located at the optimum interatomic distance r_0.

A, B, p, and q are fitting parameters, which have to be determined for each atom combination. In order to describe the cluster-surface interaction, the six interatomic potentials V(Mo−Mo), V(S−S), V(Au−Au), V(Mo−S), V(Mo−Au), and V(Au−S) were generated. The fitting was performed with respect to potential energy curves calculated by full DFT for small reference structures like the dimer, trimers and tetramers. For the Au-Au interaction potential also the data of DFT slab calculations were included in the data base for the fit. The bond-specific values for the parameters A, B, p, and q are listed in Table 1. A Fermi-type cutoff function was used to smoothly confine the interatomic interactions within the nearest neighbour sphere, thus, the V(S−S) pair potential does not contribute to the cluster-surface interaction.

With binding energies of −3.47 eV for the bridge position, −3.17 eV for the hollow site positions and −2.84 eV

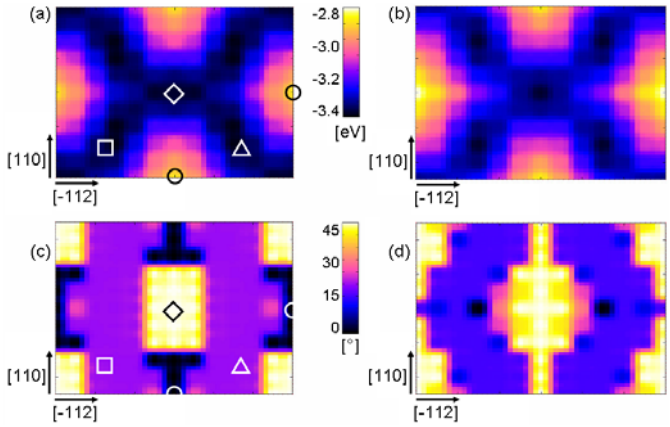

Fig. 6. (Color online) Comparison of the potential energy surfaces calculated by full DFT (left panels) and with the classical model potentials (right panels). Panels (a) and (b) give the binding energy [eV] as a function of the position of the cluster on the surface, panels (c) and (d) give the corresponding rotation angle ϕ of the square around an axis parallel to the surface normal. For $\phi = 0$ two edges of the square are parallel to a $\langle 111 \rangle$ direction.

for the on-top position the description by of the interaction by classical potentials reproduces very well the binding energies for the unrelaxed cluster calculated at the LDA level (-2.74 to -3.47 eV). The calculated cluster-surface distances at the DFT-optimised high-symmetry positions were included in the data set for the parameter optimisation of the Gupta potentials, hence, the cluster-surface distances of the most stable positions are reproduced by the classical potentials.

The analysis of the potential energy hypersurface given in Section 4.2 focuses on the lateral translation state at the optimum rotation angle ϕ around the surface normal and the energy barriers to be overcome between adjacent minima. However, the low-energy transition path between two such minima also involves a rotation around the angle ϕ, which must not be neglected when studying the motion of a Mo_6S_8 cluster on the Au(111) surface. Thus, the potential energy surface as a function of the lateral cluster motion on the Au(111) surface has been complemented by the corresponding angle distribution plot. Figure 6 provides this information: panel (a) shows the binding energy landscape as obtained from the full DFT treatment of a regular monolayer of Mo_6S_8 clusters as described above in Section 4.2; panel (b) displays the corresponding binding energy calculated with the model potentials for a single Mo_6S_8 cluster on the Au(111) surface. The lower part of Figure 6 gives the corresponding angle distributions for the rotation of the cluster around the axis parallel to the surface normal, in (c) for the full DFT, in (d) for the classical modelling. For $\phi = 0$ two edges of the square are parallel to a $\langle 111 \rangle$ direction of the surface.

The comparison yields two major results of importance for the description of the self-assembly process. First, the extrema and the saddle points of the potential energy surfaces (a) and (b) are in very good agreement, although the saddle point geometries and energies were not included in the data used for the potential fitting. Hence, the thermodynamics of the cluster adsorption is well represented in the classical picture. Differences between the plots (a) and (b) occur in the close vicinity of the minima, where the classical modelling overestimates the curvature and pins the cluster more strongly to the optimum positions. This deviation is not crucial, because the cluster deposition and self-assembly dynamics of interest here is a high-temperature process dominated by the translational and rotational motion of the cluster. Only the low-temperature dynamics of localised clusters would be dominated by the vibrational degrees of freedom, which were neglected in the classical model for the sake of simplicity.

Second, the angle distributions calculated by DFT (panel (c)) and by classical modelling (panel (d)) fully agree at the low-energy positions and exhibit an average deviation of only up to five degrees around the saddle points between those minima. Thus, the classical model reproduces the trajectory of the cluster inside the potential well of the surface almost quantitatively. The only pronounced deviation occurs for the rotation state at the most unfavourable `square on-top` position. As this global maximum is 0.6 eV higher than the global minimum and at least 0.3 eV higher than the highest transition state, this discrepancy will not play a role in modelling the coverage of Au(111) by Mo_6S_8 clusters with classical potentials.

6 Conclusions

The structural properties and the adsorption energetics of the Mo_6S_8 cluster on the Au(111) surface was investigated by density-functional band-structure calculations, employing pseudopotentials and a plane-wave basis set. The most stable adsorption occurs via a face of the cuboid cluster, such that the central molybdenum atom of the lower Mo_6S_8 face is located at the `bridge` site between two adjacent gold atoms. The four sulphur atoms of the face occupy on-top or bridge-type sites of the surface. The Mo_6S_8 cluster is bound on the gold surface with 4.07 eV at the LDA level. The two different three-fold coordinated hollow-site positions are isoenergetic, hence the cluster-surface interaction is mainly limited to the first layer of surface atoms, and the presence or absence of a gold atom in the subsurface layer is not important. In general, the Mo-Au and S-Au distances tend to the values obtained from an addition of the corresponding covalent radii. An adsorption via only one sulphur atom is less favourable by about 1 eV with respect to the `square` orientation.

The potential energy surface has an extended well of degenerate local minima, which are separated by energy barriers lower than 0.3 eV. A Bader analysis of the electronic structure revealed no net ionic contribution to the cluster-surface interaction. Thus, the cluster-surface interaction has been modelled successfully by classical pair potentials of the Gupta type. Within the temperature range relevant for the deposition and assembly processes the potential energy hypersurface calculated with these classical

potentials reflects all properties of the one obtained from full DFT calculations.

In conclusion, the Mo_6S_8 cluster exhibits all prerequisites as building block for the formation of stable and well-organised inorganic monolayers on a gold substrate. Such strongly bound, but regular inorganic monolayers are very important interface-active agents, which enhance the wettability of the otherwise poorly wettable noble metal gold by ionic compounds or which provide a structured template for the ordered adsorption of biological substances.

The authors acknowledge financial support by the Deutsche Forschungsgemeinschaft, via SPP 1153.

References

1. Z.R. Zhou, L. Vincent, Wear **229**, 962 (1999)
2. M.D. Levi, D. Aurbach, J. Power Sources **146**, 349 (2005)
3. J.V. Lauritsen, J. Kibsgaard, S. Helveg, H. Topsoe, B.S. Clausen, E. Laegsgaard, F. Besenbacher, Nature Nanotech. **2**, 53 (2007)
4. Y.R. Hacohen, R. Popovits-Biro, Y. Prior, S. Gemming, G. Seifert, R. Tenne, Phys. Chem. Chem. Phys. **5** 1644 (2003)
5. N. Bertram, Y.D. Kim, G. Ganteför, Appl. Phys. A (to be published)
6. S. Gemming, G. Seifert, Appl. Phys. A **82**, 175 (2006)
7. S. Gemming, G. Seifert, Novel Elongated Molybdenum Sulfide Nanostructures in *Proc. 19th International Winterschool on Electronic Properties of Novel Materials*, AIP Conf. Proc. **786**, 353 (2005)
8. E.H.K. et al., Am. Inst. Phys. **786**, 353 (2005)
9. N. Bertram, Y.D. Kim, G. Gantefor, Q. Sun, P. Jena, J. Tamuliene, G. Seifert, Chem. Phys. Lett. **396**, 341 (2004)
10. G. Seifert, J. Tamuliene, S. Gemming, Comp. Mat. Sci. **35**, 316 (2006)
11. X.D. Wen, T. Zeng, Y.W Li, J. Wang, H. Jiao, J. Phys. Chem B **109**, 18491 (2005)
12. M. Brändle, G. Calzaferri, M. Lanz, Chem. Phys. **201**, 141 (1995)
13. P. Murugan, V. Kumar, Y. Kawazoe, N. Ota, Phys. Rev. A **71**, 063203 (2005)
14. W. Zhang, X. Ran, H. Zhao, L. Wang, J. Chem. Phys. **121**, 7717 (2004)
15. R.P. Diez, Int. J. Quant. Chem. **76**, 105 (2000)
16. V. Koteski, B. Cekić, N. Novaković, J. Beloševic-Čavor, Mater. Sci. Forum **494**, 79 (2005)
17. D. Salloum, R. Gautier, P. Gougeon, M. Potel, Sol. St. Chem. **177**, 1672 (2004)
18. S. Picard, D. Salloum, P. Gougeon, M. Potel, Acta Cryst. **C60**, i61 (2004)
19. J.M. Lightstone, M.J. Patterson, M.G. White, Chem. Phys. Lett. **413**, 429 (2005)
20. X.-D. Wen, T. Zeng, B.-T. Teng, F.-Q. Zhang, Y.-W. Li, J. Wang, H. Jiao, J. Mol. Cat. A **249**, 191 (2006)
21. M.V. Bollinger, J.V. Lauritsen, K.W. Jacobsen, J.K. Norskov, S. Helveg, F. Besenbacher, Phys. Rev. Lett. **87**, 196803 (2001)
22. H. Topsoe, B. Hinnemann, J.K. Norskov, J.V. Lauritsen, F. Besenbacher, P.L. Hansen, G. Hytoft, R.G. Egeberg, K.G. Knudesen, Catal. Today **107**, 12 (2005)
23. M. Bar-Sadan, A.N. Enyashin, S. Gemming, R. Popovits-Biro, S. Y. Hong, Y. Prior, R. Tenne, G. Seifert, J. Phys. Chem. B **110**, 25399 (2006)
24. A. N. Enyashin, S. Gemming, M. Bar-Sadan, R. Popovits-Biro, S.Y. Hong, Y. Prior, R. Tenne, G. Seifert, Ang. Chem. Int. Ed. **46**, 623 (2007)
25. G. Seifert, H. Terrones, M. Terrones, G. Jungnickel, T. Frauenheim, Phys. Rev. Lett. **85**, 146 (2000)
26. R. Tenne, Nature Nanotech. **1**, 103 (2006)
27. S. Gemming, G. Seifert, I. Vilfan, Phys. Stat. Sol. B **243**, 3320 (2006)
28. J. Kristensen, J. Zhang, I. Chorkendorff, J. Ulstrup, B.L. Ooi, Dalton Trans., 3985,(2006)
29. J.M. Lightstone, M.J. Patterson, J. Lofaro, P. Liu, M.G. White, *Proc. XIII International Symposium on Small Particles and Inorganic Clusters*, Göteborg University, Sweden, 2006, p. 155
30. M.M. Biener, J. Biener, R. Schalek, C.M. Friend, Surf. Sci. **594**, 221 (2005)
31. D.V. Potapenko, J.M. Horn, R.J. Beuhler, Z. Song, M.G. White, Surf. Sci. **574**, 244 (2005)
32. The ABINIT code is a common project of the Universite Catholique de Louvain, Corning Incorporated, and other contributors (`URL http://www.abinit.org`)
33. P. Hohenberg, W. Kohn, Phys. Rev. **136**, B864 (1964)
34. W. Kohn, L. Sham, Phys. Rev. **140**, 1133 (1965)
35. N. Troullier, J. Martins, Phys. Rev. B **43**, 8861 (1991)
36. J.P. Perdew, K. Burke, M. Ernzerhof, Phys. Rev. Lett. **77**, 3865, (1996)
37. R.W.F. Bader, *Atoms in Molecules: A Quantum Theory* (Oxford University, NY, 1994)
38. J.E. Huheey, E.A. Keiter, R.L. Keiter, *Inorganic Chemistry: Principles of Structure and Reactivity*, 4th edn. (HarperCollins, New York, USA, 1993)
39. S. Gemming, G. Seifert, Nature Nanotech. **2**, 22 (2007)